Low-Complexity Maximum-Likelihood Detector for IoT BLE Devices

Jose Valencia-Velasco, *Member, IEEE*, Omar Longoria-Gandara, *Member, IEEE*, Rodrigo Aldana-Lopez, *Member, IEEE*, and Luis Pizano-Escalante, *Member, IEEE*

***Abstract*—Internet of Things (IoT) is a technology that has overgrown and whose interest lies in the connection of diverse kinds of devices to collect and exchange data. Since most IoT devices are mobile, the hardware resources are hard limited; thus, complexity reduction becomes a relevant concern in this context. Bluetooth low energy (BLE) communication standard has an important position in IoT due to its Gaussian frequency-shift keying (GFSK) modulation scheme employed in the physical layer, which provides both attractive spectral and power efficiency. Typically, GFSK requires a maximum-likelihood sequence estimator (MLSE) implemented through the Viterbi algorithm (VA) at the receiver. This article provides a GFSK receiver based on a new paradigm that transforms the I-Q baseband signal and uses the VA with a reduced-complexity proposed metrics. Comparisons of theoretical and simulated results are presented, and they show that the proposed metrics for the GFSK receiver are compliant with the Bluetooth standard. Henceforth, the proposed receiver is an attractive scheme for IoT BLE devices.**

***Index Terms*—Bluetooth, digital modulation, Gaussian frequency-shift keying (GFSK), Internet of Things (IoT), low energy, Viterbi algorithm (VA).**

I. Introduction

THE Internet of Things (IoT) is a leading-edge technology which allows connecting a variety of devices for automotive infotainment, medical healthcare, home automation, and machine-to-machine (M2M) communications, with the purpose of interchange information without human intervention [1], [2]. Among the wide range of communication protocols/standards used by these devices, Bluetooth low energy (BLE) has gained special attention due to its low energy consumption [3], [4].

The BLE core specification establishes Gaussian frequency-shift keying (GFSK) as the modulation scheme at the physical layer [5]. GFSK is a subclass of continuous phase modulation (CPM) whose main features are a constant envelope, which overcomes nonlinear amplitude distortion in the power amplifier and high spectral efficiency.

Manuscript received October 3, 2019; revised December 20, 2019; accepted January 6, 2020. Date of publication January 17, 2020; date of current version June 12, 2020. *(Corresponding author: Jose Valencia-Velasco.)*

Jose Valencia-Velasco, Omar Longoria-Gandara, and Luis Pizano-Escalante are with the Department of Electronics, Systems and IT, Instituto Tecnológico y de Estudios Superiores de Occidente, Tlaquepaque 45604, Mexico (e-mail: ng100357@iteso.mx; olongoria@iteso.mx; luispizano@iteso.mx).

Rodrigo Aldana-Lopez is with the Department of Computer Science and Systems Engineering, University of Zaragoza, 50018 Zaragoza, Spain (e-mail: 794214@unizar.es).

Digital Object Identifier 10.1109/JIOT.2020.2966988

Regarding the detection process of GFSK, the optimal receiver uses a maximum-likelihood sequence estimator (MLSE). However, its implementation requires a high amount of hardware resources (e.g., memory and processing units), which are limited in IoT platforms.

The Viterbi algorithm (VA) can be used as a sequence detector because it reduces the number of sequences in the search as new data arrives at the receiver [6], [7]. Even though the VA is less computationally expensive than the exhaustive search employed by the MLSE, unfortunately, its hardware implementation is still unfeasible for most IoT applications. Likewise, other approaches, such as [8]–[10] use symbol-by-symbol detectors with a considerable low complexity at expenses of severe performance degradation.

In this context, the reduction of implementation complexity while maintaining a performance close to the MLSE is a research problem of particular interest. Henceforth, we consider the following two approaches: the first one consists of a GFSK signal simplification. In contrast, the second approach relies on the simplification or reduction in the number of operations required to perform the VA implementation.

Regarding the first approach, [11] proposes a GFSK receiver based on Rimoldi's decomposition of the GFSK signal with a performance loss of 2 dB with respect to MLSE at a bit error rate (BER) of 10^{-3} and modulation index of $1/3$. Moreover, Ibrahim *et al.* [12] presented a GFSK receiver based on Laurent's decomposition of the GFSK signal and a decision feedback equalizer, obtaining a loss of 0.5 dB with respect to [11] while reducing the complexity of the receiver.

Likewise, to address the second approach, i.e., the reduction in the number of operations required in the VA implementation, in [13], an approach that simplifies the realization of VA is introduced.

A. Objectives and Contributions

This article provides a GFSK receiver based on a new paradigm that transforms the I (in-phase) and Q (quadrature) components of the baseband signal and uses the VA with a reduced-complexity proposed metrics. Since most IoT devices are mobile, the hardware resources are hard limited; thus, complexity reduction becomes a relevant concern in this context. Under these circumstances, the proposals are very engaging since less memory and arithmetic blocks are required, which means a complexity reduction in hardware implementation. Likewise, theoretical and simulated results, under the

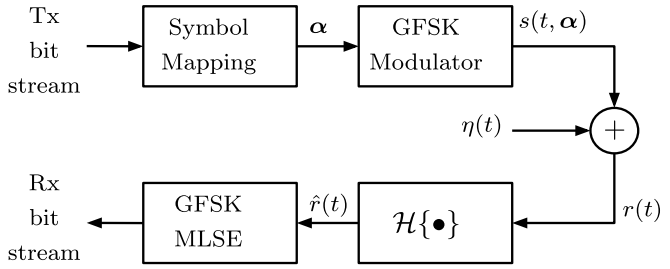

Fig. 1. Proposed block diagram of a GFSK wireless communication system.

additive white Gaussian noise (AWGN) channel, corroborate the evidence that the proposals comply BLE performance in terms of BER [5].

B. Organization

This article is organized as follows. Section II describes in detail the signal model. Section III presents the design of the proposed low-complexity receiver. In Section IV, the theoretical error performance is obtained. Meanwhile, the simulation results are presented and discussed in Section V. Finally, the conclusions are drawn in Section VI.

II. GFSK Signal Model

Fig. 1 shows the GFSK communication system employed in this article. Each block will be discussed in the following sections as is required.

The input bit stream is mapped to symbols $\alpha_i \in \{+1, -1\}$ and the GFSK modulator takes N symbols represented by $\boldsymbol{\alpha} = \{\alpha_0, \alpha_1, \alpha_2, \ldots, \alpha_{N-1}\}$, which generates the complex envelope of a GFSK signal described by

$$s(t, \boldsymbol{\alpha}) = \sqrt{E_s/T} \exp\{j\phi(t, \boldsymbol{\alpha})\} \tag{1}$$

where

$$\phi(t, \boldsymbol{\alpha}) = 2\pi h \sum_{i=0}^{k} \alpha_i q(t - iT), \quad kT \le t < (k+1)T \tag{2}$$

is the phase signal, h represents the modulation index, T is the symbol time interval, and E_s is the energy of a symbol during an interval of length T, and obtained by

$$\int_t^{t+T} \|s(\tau, \boldsymbol{\alpha})\|^2 d\tau = \frac{E_s}{T} \int_t^{t+T} d\tau = E_s.$$

The phase pulse shaping $q(t)$ employed in (2), with duration of L symbol periods, is described as

$$q(t) = \int_0^t g(\tau) d\tau \tag{3}$$

where $g(t)$ is the Gaussian pulse given by

$$g(t) = \frac{1}{2T}\left[Q\left(2\pi BT\left(\frac{t - T/2}{\sqrt{\ln(2)}T}\right)\right) - Q\left(2\pi BT\left(\frac{t + T/2}{\sqrt{\ln(2)}T}\right)\right)\right] \tag{4}$$

with BT representing the bandwidth-time product (specified as $BT = 0.5$ for Bluetooth) and $Q(\bullet)$ denoting the complementary error function.

Splitting the phase signal (2) in two contributions

$$\phi(t, \boldsymbol{\alpha}) = 2\pi h \sum_{i=k-L+1}^{k} \alpha_i q(t - iT) + 2\pi h \sum_{i=0}^{k-L} \alpha_i q(t - iT) \tag{5}$$

and considering that $q(t)$ has a maximum value of $1/2$ for $t > LT$, as is shown in [14, Fig. 6.2], the second contribution can be simplified; thus, (5) can be rewritten as

$$\phi(t, \boldsymbol{\alpha}) = 2\pi h \sum_{i=k-L+1}^{k} \alpha_i q(t - iT) + \pi h \sum_{i=0}^{k-L} \alpha_i \bmod 2\pi = \theta(t, \alpha_k, \ldots, \alpha_{k-L+1}) + \theta_k, \quad kT \le t < (k+1)T \tag{6}$$

where $\theta(t, \alpha_k, \ldots, \alpha_{k-L+1})$ is the phase contribution in $[kT, (k+1)T]$ and θ_k represents the cumulative phase up to time $(k-L)T$.

In the case of GFSK, with $h = 0.5$, $BT = 0.5$, and a partial response of $L = 3$, the complex envelope signal results in

$$s(t, \boldsymbol{\alpha}) = \sqrt{E_s/T} \exp\{j\pi(\alpha_k q(t - kT) + \alpha_{k-1} q(t - (k-1)T) + \alpha_{k-2} q(t - (k-2)T)) + j\theta_k\}. \tag{7}$$

For BLE systems, the core specification [5] defines a bandwidth of 2 MHz, and some research studies [15], [16] have shown that the communication channel for such systems can be assumed as the flat-fading channel (nonfrequency selective) [17, Ch. 4]. In order to combat the multipath fading, the Bluetooth core specification [5] establishes the technique of adaptive frequency hopping; the effectiveness of this technique is demonstrated clearly in [18]. Henceforth, for baseband communications of BLE systems, the AWGN channel can be assumed to evaluate the system performance [19].

Now, considering that the signal (7) is transmitted over a Gaussian noise channel, the received baseband signal, $r(t)$, can be described as

$$r(t) = s(t, \boldsymbol{\alpha}) + \eta(t) \tag{8}$$

where $\eta(t)$ is a zero-mean additive complex white Gaussian noise with variance $\sigma^2 = N_0/2$ per real and imaginary components and power spectral density of $N_0/2$.

III. GFSK Low-Complexity Receiver Design

This section summarizes the metrics proposed in [1], where the I and Q components of the baseband signal [1, Fig. 3], at the receiver end, are quantized with the values -1 and $+1$. This is obtained by the uniform quantization of the phase signal, $\phi(t, \boldsymbol{\alpha})$, with step size $\pi/2$ and offset $\pi/4$, as follows:

$$\hat{\phi}(t, \boldsymbol{\alpha}) = \frac{\pi}{2}\left\lfloor \frac{2}{\pi}\phi(t, \boldsymbol{\alpha}) \right\rfloor + \frac{\pi}{4} \tag{9}$$

TABLE I
QUANTIZED PHASE SIGNAL, $\hat{\phi}(t,\boldsymbol{\alpha})$, VALUES FROM (9)

Phase signal $\phi(t,\boldsymbol{\alpha})$	$\hat{\phi}(t,\boldsymbol{\alpha})$	$\text{sign}(\cos(\phi(t,\boldsymbol{\alpha})))$	$\text{sign}(\sin(\phi(t,\boldsymbol{\alpha})))$
$[0,\frac{\pi}{2})$	$\frac{\pi}{4}$	$+1$	$+1$
$[\frac{\pi}{2},\pi)$	$\frac{3\pi}{4}$	-1	$+1$
$[\pi,\frac{3\pi}{2})$	$\frac{5\pi}{4}$	-1	-1
$[\frac{3\pi}{2},2\pi)$	$\frac{7\pi}{4}$	$+1$	-1

where $\lfloor\cdot\rfloor$ is the floor operation. The corresponding complex envelope of the quantized phase signal is obtained in [1] and described as

$$\hat{s}(t,\boldsymbol{\alpha}) = \sqrt{E_s/T}\exp\left\{j\hat{\phi}(t,\boldsymbol{\alpha})\right\} = \sqrt{\frac{E_s}{2T}}(\text{sign}(\cos(\phi(t,\boldsymbol{\alpha}))) + j\,\text{sign}(\sin(\phi(t,\boldsymbol{\alpha})))) \quad (10)$$

with

$$\text{sign}(x) = \begin{cases} +1, & \text{if} \quad x \geq 0 \\ -1, & \text{if} \quad x < 0. \end{cases} \quad (11)$$

This motivates the introduction of the following operator:

$$\mathcal{H}\{\bullet\} = \sqrt{E_s/T}(\text{sign}(\text{Re}\{\bullet\}) + j\,\text{sign}(\text{Im}\{\bullet\})). \quad (12)$$

Hence, (10) can be expressed as $\hat{s}(t,\boldsymbol{\alpha}) = \mathcal{H}\{s(t,\boldsymbol{\alpha})\}$ and with reference to Fig. 1, $\hat{r}(t) = \mathcal{H}\{r(t)\}$, which corresponds to the transformation of the received signal $r(t)$ according to (12). In this way, $\hat{r}(t)$ takes values in a finite set of $\sqrt{E_s/T}\{1+j, 1-j, -1+j, -1-j\}$.

A. Quantized Phase GFSK as QPSK Modulation

This section shows that (10) can be represented as a quadrature phase shift-keying (QPSK) baseband signal. Note that from (9) and according to Table I, $\hat{\phi}(t,\boldsymbol{\alpha})$ mod 2π can only take values in $\{\pi/4, 3\pi/4, 5\pi/4, 7\pi/4\}$. Therefore, by expanding all possible values of (9) in terms of $\alpha_k, \alpha_{k-1}, \alpha_{k-2}$, and θ_k the following relation is obtained:

$$\hat{\phi}_k := \hat{\phi}(t,\boldsymbol{\alpha}) = \frac{\pi}{2}\Theta_k + \frac{\pi}{4}, \quad kT \leq t < (k+1)T$$
$$\Theta_k = \frac{1}{2}(\alpha_k + \alpha_{k-1}) + \Theta_{k-1} \quad (13)$$

with $\Theta_{-1} = 0$. These conditions can be sumarized by the following: the phase $\hat{\phi}_k$ increases with respect to $\hat{\phi}_{k-1}$ if

$$\alpha_k = \alpha_{k-1} = 1 \quad (14)$$

decreases if

$$\alpha_k = \alpha_{k-1} = -1 \quad (15)$$

and stays the same if

$$\alpha_k \neq \alpha_{k-1}. \quad (16)$$

Henceforth, (10) can be rewritten as

$$\hat{s}(t,\boldsymbol{\alpha}) = \sqrt{E_s/T}\exp\left(j\hat{\phi}_k\right), \quad kT \leq t < (k+1)T$$
$$\hat{\phi}_k \text{ mod } 2\pi \in \{\pi/4, 3\pi/4, 5\pi/4, 7\pi/4\} \quad (17)$$

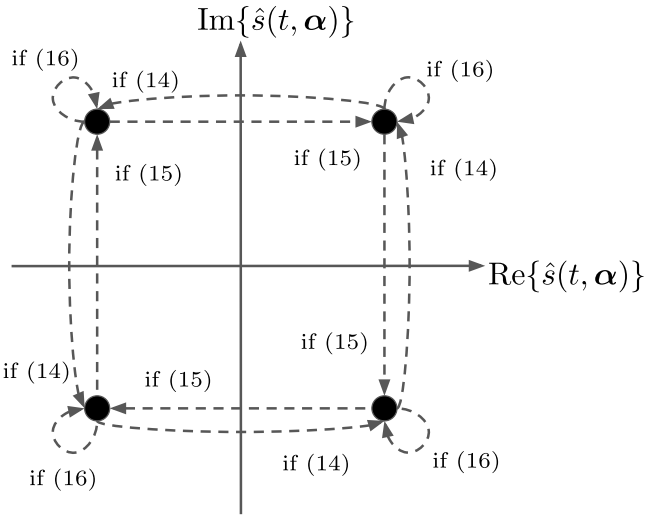

Fig. 2. State transitions for $\hat{s}(t,\boldsymbol{\alpha})$ from an interval $(k-1)T \leq t < kT$ to $kT \leq t < (k+1)T$.

which is a representation of a $\pi/4$-QPSK signal where the input sequence of symbols $\boldsymbol{\alpha}$ are encoded through the state machine to obtain the new sequence of 4-ary symbols $\{\hat{\phi}_0, \ldots, \hat{\phi}_{N-1}\}$. The phase transitions are represented graphically in Fig. 2.

B. State Trellis Diagram

The GFSK signal (7) is given by three contributions: 1) the transmitted symbol α_k; 2) the correlative state vector $(\alpha_{k-1}, \alpha_{k-2})$; and 3) the phase memory θ_k. Thus, it can be represented by the total state vector $\boldsymbol{\sigma}_k = (\theta_k, \alpha_{k-1}, \alpha_{k-2})^T$ and the symbol α_k.

From the definition of the accumulated phase θ_k in (6), where θ_k is equal to $[\pi h \sum_{i=0}^{k-L}\alpha_i]$ mod 2π, it follows that $\theta_{k+1} = \alpha_{k-2}(\pi/2) + \theta_k$. Hence, the transition rule of the total state vector $\boldsymbol{\sigma}_k$ over the time intervals can be represented by the following vector equation:

$$\boldsymbol{\sigma}_{k+1} = \begin{pmatrix} 1 & 0 & \pi/2 \\ 0 & 0 & 0 \\ 0 & 1 & 0 \end{pmatrix}\boldsymbol{\sigma}_k + \begin{pmatrix} 0 \\ 1 \\ 0 \end{pmatrix}\alpha_k. \quad (18)$$

Note that since θ_k can only take values in $\{0, \pi/2, \pi, 3\pi/2\}$ for $h = 0.5$, there are 16 possible combinations for $\boldsymbol{\sigma}_k$ *when taking into account only* θ_k mod 2π. Therefore, the state trellis diagram can be constructed using the possible states of $\boldsymbol{\sigma}_k$ and the transition rule (18), as it is shown in Fig. 3. The trellis diagram is extended for T_b intervals, where T_b is known as the traceback, so that the goal is to estimate the sequence $\alpha_k, \ldots, \alpha_{k+T_b-1}$. A well-known estimation algorithm is the VA [20], which obtains the MLSE. The received signal is compared with a reference signal in a certain path along the trellis using a likelihood metric. The MLSE is chosen to be the path with the best metric value. Ideally, the traceback value would be large enough to cover the entire received sequence. In practice, a heuristic is applied and T_b can be reduced up to

$$T_b = 5\log_2(N_s) \quad (19)$$

where $N_s = 16$ is the number of possible states in the trellis diagram.

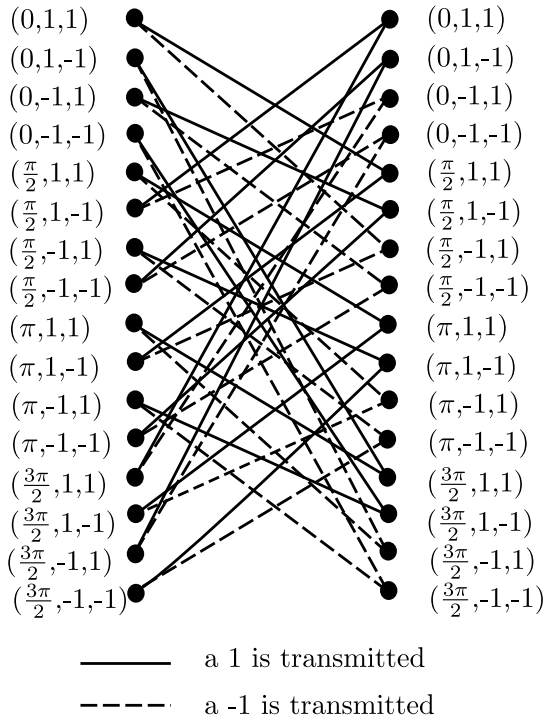

Fig. 3. Trellis diagram for a GFSK signal with modulation index of 0.5 and pulse length of three symbol periods.

C. Traditional Metric

Traditionally, the metric used in the VA for CPM signals, is calculated as the Euclidean distance [6, eq. (4.8-1)] between the received signal $r(t)$ and the reference signal considering $\boldsymbol{\sigma}_k$ and α_k

$$J_k(\alpha_k, \boldsymbol{\sigma}_k) = \frac{T}{E_s} \int_{kT}^{(k+1)T} \|r(t) - S(t, \alpha_k, \boldsymbol{\sigma}_k)\|^2 dt \quad (20)$$

where $S(t, \alpha_k, \boldsymbol{\sigma}_k)$ is the reference signal defined as

$$\begin{aligned} S(t, \alpha_k, \boldsymbol{\sigma}_k) &= \sqrt{E_s/T} \exp(j\Phi(t, \alpha_k, \boldsymbol{\sigma}_k)) \\ \Phi(t, \alpha_k, \boldsymbol{\sigma}_k) &= \pi\alpha_k q(t - kT) + \alpha_{k-1} q(t - (k-1)T) \\ &\quad + \alpha_{k-2} q(t - (k-2)T) + \theta_k. \end{aligned}$$

Thus, the discrete-time version of (20) is described as

$$\overline{J_k}(\alpha_k, \boldsymbol{\sigma}_k) = \frac{T}{E_s} \sum_{n=M_p k}^{M_p(k+1)-1} \|r(n) - S(n, \alpha_k, \boldsymbol{\sigma}_k)\|^2 \quad (21)$$

where the signal is sampled at a rate of M_p samples per symbol. Note that this approach requires the storing of all the reference sequences $S(n, \alpha_k, \boldsymbol{\sigma}_k)$ in memory in order to compute the MLSE path. Furthermore, the samples should be represented with a given precision which can be called a single *word* without loss of generality. The size of the *word* defines the size of the adders, subtractors, and multipliers required to implement (21).

D. Metric Proposal 1

The Euclidean distance between the signal $\hat{r}(t) \in \sqrt{E_s/T}\{1 + j, 1 - j, -1 + j, -1 - j\}$ and the reference signal is computed by

$$J_k(\alpha_k, \boldsymbol{\sigma}_k) = \frac{T}{E_s} \int_{kT}^{(k+1)T} \left\|\hat{r}(t) - S(t, \alpha_k, \boldsymbol{\sigma}_k)\right\|^2 dt. \quad (22)$$

A discrete-time version of (22) is given by

$$\overline{J_k}(\alpha_k, \boldsymbol{\sigma}_k) = \frac{T}{E_s} \sum_{n=M_p k}^{M_p(k+1)-1} \left\|\hat{r}(n) - S(n, \alpha_k, \boldsymbol{\sigma}_k)\right\|^2. \quad (23)$$

Note that in this metric, the real and imaginary components of $\sqrt{(T/E_s)}\hat{r}(n)$ can only be 1 or -1. Therefore, the computational complexity of (23) is reduced if the following precomputed signals are stored in memory:

$$\begin{aligned} D_1(n, \alpha_k, \boldsymbol{\sigma}_k) &= \left\|(+1 + j) - \sqrt{\frac{T}{E_s}} S(n, \alpha_k, \boldsymbol{\sigma}_k)\right\|^2 \\ D_2(n, \alpha_k, \boldsymbol{\sigma}_k) &= \left\|(-1 + j) - \sqrt{\frac{T}{E_s}} S(n, \alpha_k, \boldsymbol{\sigma}_k)\right\|^2 \\ D_3(n, \alpha_k, \boldsymbol{\sigma}_k) &= \left\|(+1 - j) - \sqrt{\frac{T}{E_s}} S(n, \alpha_k, \boldsymbol{\sigma}_k)\right\|^2 \\ D_4(n, \alpha_k, \boldsymbol{\sigma}_k) &= \left\|(-1 - j) - \sqrt{\frac{T}{E_s}} S(n, \alpha_k, \boldsymbol{\sigma}_k)\right\|^2. \end{aligned} \quad (24)$$

Consequently, a sample of one of these signals is selected depending on the signs of the real and imaginary part of $\hat{r}(n)$, saving multiplication and subtraction operations, and leaving only *word*-sized additions, but requiring four times memory locations with respect to the traditional metric described in (20).

E. Metric Proposal 2

An alternative metric is given by comparing $\hat{r}(n)$ with a reference signal $\hat{S}(t, \alpha_k, \boldsymbol{\sigma}_k) = \mathcal{H}\{S(t, \alpha_k, \boldsymbol{\sigma}_k)\}$

$$J_k(\alpha_k, \boldsymbol{\sigma}_k) = \frac{T}{4E_s} \int_{kT}^{(k+1)T} \left\|\hat{r}(t) - \hat{S}(t, \alpha_k, \boldsymbol{\sigma}_k)\right\|^2 dt. \quad (25)$$

A discrete-time version of (25) is computed with

$$\overline{J_k}(\alpha_k, \boldsymbol{\sigma}_k) = \frac{T}{4E_s} \sum_{n=M_p k}^{M_p(k+1)-1} \left\|\hat{r}(n) - \hat{S}(n, \alpha_k, \boldsymbol{\sigma}_k)\right\|^2. \quad (26)$$

This simplifies the required precision for the samples, since both $\hat{r}(n)$ and $\hat{S}(n, \alpha_k, \boldsymbol{\sigma}_k)$ can be represented using just 2 bits for each one. For instance, let $\{r_R\ r_I\}$ represent $\hat{r}(n)$ and $\{S_R\ S_I\}$ represent $\hat{S}(n, \alpha_k, \boldsymbol{\sigma}_k)$, e.g., $\{r_R\ r_I\} = \{0\ 1\}$ corresponds to $\sqrt{(T/E_s)}\hat{r}(n) = 1 - j$. Furthermore, the result of $(T/4E_s)\|\hat{r}(n) - \hat{S}(n, \alpha_k, \boldsymbol{\sigma}_k)\|^2$ can only be 0, 1, or 2 and is represented using 2 bits as well $\{b_1\ b_2\}$, where $\{0\ 0\}$ corresponds to 0, $\{0\ 1\}$ to 1, and $\{1\ 0\}$ to 2. The relationship between $\{r_R\ r_I\ S_R\ S_I\}$ and $\{b_1\ b_2\}$ can be computed by a lookup table or with the Boolean equations

$$\begin{aligned} b_1 &= (r_R \oplus S_R) \odot (r_I \oplus S_I) \\ b_2 &= (r_R \oplus S_R) \oplus (r_I \oplus S_I) \end{aligned} \quad (27)$$

TABLE II
COMPARISON OF HARDWARE RESOURCES BETWEEN THE PROPOSED METRICS

Metric	Bus size	Adders	Subs.	Mult.	Memory
Trad. → (21)	1 word	$M_p - 1$	M_p	M_p	$2N_sM_p$ words
Prop. 1 → (23)	1 word	$M_p - 1$	0	0	$8N_sM_p$ words
Prop. 2 → (26) or (28)	$2 + \log_2(M_p)$ bits	$M_p - 1$	0	0	$4N_s$ bits

TABLE III
HARDWARE RESOURCES CONSIDERING IEEE-754 SINGLE PRECISION, $M_p = 20$ AND $N_s = 16$

Scheme	Bus size (bits)	Adders	Subs.	Mult.	Memory (bits)
Traditional	32	19	20	20	20,480
Proposal 1	32	19	0	0	81,920
Proposal 2	7	19	0	0	64

where $\oplus$ and $\odot$ stands for XOR and AND logical operations, respectively. With these two bits, the values 0, 1, or 2 are added to the metric described in (26). Moreover, the amount of memory is reduced since only two bits are needed to store $\hat{S}(n, \alpha_k, \boldsymbol{\sigma}_k)$, resulting in a total of $2(2N_s)$ bits considering all states. Furthermore, the adder bus size is reduced since in the worst case, the metric results in $2M_p$, which require $2 + \log_2(M_p)$ bits to be represented.

Note that (26) turns out equivalent to the following metric:

$$\overline{J_k}(\alpha_k, \boldsymbol{\sigma}_k) = \sqrt{\frac{T}{2E_s}} H_k\Big(\mathrm{Re}\big\{\hat{r}(n)\big\}, \mathrm{Re}\Big\{\hat{S}(n, \alpha_k, \boldsymbol{\sigma}_k)\Big\}\Big) + H_k\Big(\mathrm{Im}\big\{\hat{r}(n)\big\}, \mathrm{Im}\Big\{\hat{S}(n, \alpha_k, \boldsymbol{\sigma}_k)\Big\}\Big) \quad (28)$$

where $H_k(\cdot, \cdot)$ is the Hamming distance operation for signals with range $\sqrt{(E_s/T)}\{1, -1\}$ and can be computed as

$$H_k(x(n), y(n)) = \sum_{n=M_pk}^{M_p(k+1)-1} |x(n) - y(n)| \quad (29)$$

which counts the amount of different samples between $x(n)$ and $y(n)$ in the interval $[M_pk, M_p(k+1) - 1]$ [21].

Table II summarizes the hardware resources for the three metrics analyzed previously. For example, Table III shows the hardware required considering the IEEE-754 single-precision standard, where each *word* is represented with 32 bits, and assuming $M_p = 20$ samples per symbol and $N_s = 16$ states in the trellis.

IV. PERFORMANCE ANALYSIS

In this section, the theoretical error performance is obtained. Symbol error probability is used as a figure of merit for performance. Assume a signal $s(t, \boldsymbol{\alpha}^i)$ encoded by the sequence of symbols $\boldsymbol{\alpha}^i$ as described in Section II. Moreover, $\boldsymbol{\alpha}^i$ is a sequence of N different symbols and therefore, there are $M = 2^N$ different possible sequences. Henceforth, the sequence error probability is defined as the probability of detecting sequence $\boldsymbol{\alpha}^j$ when the sequence $\boldsymbol{\alpha}^i$ with $j \neq i$ was transmitted. This can be described precisely by defining the following events. Let the event of transmitting a sequence $\boldsymbol{\alpha}^i$ be represented as E_T^i and the event of detecting at the receiver a sequence $\boldsymbol{\alpha}^j$ be represented as E_R^j. Therefore, an error is defined as the event $E_T^i \cap E_R^j$ with $j \neq i$ and the error probability is the probability of the union of all possible error events

$$P_e = P\left(\bigcup_{i=1}^{M} \bigcup_{j \neq i} E_T^i \cap E_R^j\right) \leq \sum_{i=1}^{M} \sum_{j \neq i} P\Big(E_T^i \cap E_R^j\Big) \quad (30)$$

where the inequality in the preceding relation follows from the well-known Boole's union inequality. Furthermore, by using the definition of conditional probability, $P(E_R^j|E_T^i)$ is the probability that the sequence $\boldsymbol{\alpha}^j$ was detected assuming that the sequence $\boldsymbol{\alpha}^i$ was transmitted. Hereafter, (30) can be expressed as

$$P_e \leq \sum_{i=1}^{M} \sum_{j \neq i} P\Big(E_R^j|E_T^i\Big) P\big(E_T^i\big). \quad (31)$$

Assuming that all M sequences have the same probability to be transmitted, then $P(E_T^i) = 1/M \ \forall \ i = 1, 2, \ldots, M$. Consequently, (31) becomes

$$P_e \leq \frac{1}{M} \sum_{i=1}^{M} \sum_{j \neq i} P\Big(E_R^j|E_T^i\Big). \quad (32)$$

In order to computing (32), note that the term $P(E_R^j|E_T^i)$ is determined by the detection process described in Section III-B, which finds the maximum-likelihood sequence for the received signal $s(t, \boldsymbol{\alpha}^i)$ based in a distance metric criterion, such as the ones described in Sections III-C, III-D, and III-E. The signals $s(t, \boldsymbol{\alpha}^j)$ $\forall j = 1, 2, \ldots, M$ belong to a signal space where distance is measured in terms of the Euclidean distance operator $\Delta\{s(t, \boldsymbol{\alpha}^i), s(t, \boldsymbol{\alpha}^j)\}$ defined as

$$\Delta\big\{s\big(t, \boldsymbol{\alpha}^i\big), s\big(t, \boldsymbol{\alpha}^j\big)\big\} = \Delta^{ij} = \sqrt{\int_0^{NT} \big\|s\big(t, \boldsymbol{\alpha}^i\big) - s\big(t, \boldsymbol{\alpha}^j\big)\big\|^2 dt}. \quad (33)$$

The Euclidean distance Δ^{ij} between two pair of signals can be expressed in terms of the difference of the encoding sequences $\boldsymbol{\gamma}^{ij} = \boldsymbol{\alpha}^i - \boldsymbol{\alpha}^j$ as

$$\begin{aligned}\big(\Delta^{ij}\big)^2 &= \int_0^{NT} \big[s\big(t, \boldsymbol{\alpha}^i\big) - s\big(t, \boldsymbol{\alpha}^j\big)\big]\big[s\big(t, \boldsymbol{\alpha}^i\big) - s\big(t, \boldsymbol{\alpha}^j\big)\big]^* dt \\ &= \int_0^{NT} \big\|s\big(t, \boldsymbol{\alpha}^i\big)\big\|^2 + \big\|s\big(t, \boldsymbol{\alpha}^j\big)\big\|^2 \\ &\quad - s\big(t, \boldsymbol{\alpha}^i\big)\big[s\big(t, \boldsymbol{\alpha}^j\big)\big]^* - s\big(t, \boldsymbol{\alpha}^j\big)\big[s\big(t, \boldsymbol{\alpha}^i\big)\big]^* dt \\ &= 2NE_s - \frac{E_s}{T} \int_0^{NT} \exp\big(j\big(\phi\big(t, \boldsymbol{\alpha}^i\big) - \phi\big(t, \boldsymbol{\alpha}^j\big)\big)\big) \\ &\quad + \exp\big(-j\big(\phi\big(t, \boldsymbol{\alpha}^i\big) - \phi\big(t, \boldsymbol{\alpha}^j\big)\big)\big) dt\end{aligned}$$

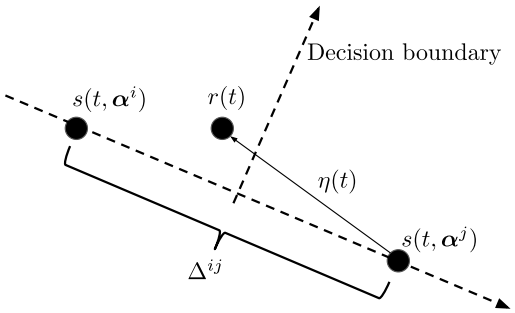

Fig. 4. Signal space representation of the received signal $r(t)$ in the AWGN channel and the decision boundary between $s(t, \boldsymbol{\alpha}^i)$ and $s(t, \boldsymbol{\alpha}^j)$.

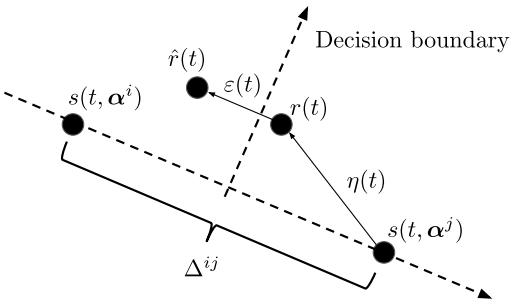

Fig. 5. Signal space representation of the received signal $r(t)$ in the AWGN channel, the signal $\hat{r}(t)$ and the decision boundary between $s(t, \boldsymbol{\alpha}^i)$ and $s(t, \boldsymbol{\alpha}^j)$.

$$= 2NE_s - \frac{2E_s}{T}\int_0^{NT} \cos\big(\phi\big(t, \boldsymbol{\alpha}^i\big) - \phi\big(t, \boldsymbol{\alpha}^j\big)\big)dt$$
$$= 2E_s\left(N - \frac{1}{T}\int_0^{NT} \cos\big(\phi\big(t, \boldsymbol{\gamma}^{ij}\big)\big)dt\right) \quad (34)$$

where $[\bullet]^*$ stands for complex conjugate. Given that $s(t, \boldsymbol{\alpha}^j)$ was transmitted, then $r(t) = s(t, \boldsymbol{\alpha}^j) + \eta(t)$ is detected as $s(t, \boldsymbol{\alpha}^i)$ when the following relation of Euclidean distance is accomplished:

$$\Delta\big\{r(t), s\big(t, \boldsymbol{\alpha}^i\big)\big\} \leq \Delta\big\{r(t), s\big(t, \boldsymbol{\alpha}^j\big)\big\}. \quad (35)$$

Consequently, an error occurs in the detection process. Therefore

$$P\Big(E_R^j | E_T^i\Big) = P\big(\Delta\big\{r(t), s\big(t, \boldsymbol{\alpha}^i\big)\big\} \leq \Delta\big\{r(t), s\big(t, \boldsymbol{\alpha}^j\big)\big\}\big). \quad (36)$$

This can be expressed in terms of the noise power in the following way. Taking as a reference Fig. 4 and choosing a coordinate system in the signal space with one axis placed from $s(t, \boldsymbol{\alpha}^i)$ to $s(t, \boldsymbol{\alpha}^j)$. Then, condition (35) is equivalent to saying that the component of $\eta(t)$ along that axis is bigger than the distance $\Delta^{ij}/2$. Therefore

$$P\Big(E_R^j | E_T^i\Big) = \int_{\Delta^{ij}/2}^{\infty} \frac{1}{\sqrt{\pi N_0}} \exp\left(\frac{\eta^2}{N_0}\right)d\eta = Q\left(\frac{\Delta^{ij}}{\sqrt{2N_0}}\right). \quad (37)$$

Hence, (32) is expressed as

$$P_e \leq \frac{1}{M}\sum_{i=1}^{M}\sum_{j\neq i} Q\left(\frac{\Delta^{ij}}{\sqrt{2N_0}}\right). \quad (38)$$

In order to obtain a tight upper bound for P_e, it is necessary to obtain the Δ^{ij} with the least distance, i.e.,

$$\Delta_{\min} = \min_{i,j \;\; i\neq j} \Delta^{ij} \quad (39)$$

since the $Q(\bullet)$ function is a monotonically decreasing function. Furthermore, K pairs of signals comply with $\Delta_{\min}$, and each pair is counted twice in the double sum. Thus, the tight upper bound for P_e in (38) is expressed as

$$P_e \leq \frac{2K}{M} Q\left(\frac{\Delta_{\min}}{\sqrt{2N_0}}\right). \quad (40)$$

Moveover, defining $d_{\min} = [(\Delta_{\min})/(\sqrt{2E_s})]$ leads to

$$P_e \leq \frac{2K}{M} Q\left(d_{\min}\sqrt{\frac{E_s}{N_0}}\right). \quad (41)$$

At this point, using (33) to calculate distances between signal encoding sequences of symbols, i.e., Δ^{ij}, is equivalent to the traditional metric described in (20). Likewise, (41) can be applied for the metric proposal 2 by changing $\Delta^{ij} = \Delta\{\hat{s}(t, \boldsymbol{\alpha}^i), \hat{s}(t, \boldsymbol{\alpha}^j)\}$.

For the case of metric proposal 1, take for instance Fig. 5, which shows that $\hat{r}(t) = s(t, \boldsymbol{\alpha}^j) + \eta(t) + \varepsilon(t)$, where $\varepsilon(t) = \hat{r}(t) - r(t)$ and represents the noise obtained by applying the operator $\mathcal{H}\{r(t)\}$. Note that the power of $\varepsilon(t)$ can be approximated by assuming $r(t)$ to be a complex exponential with period T, hence

$$\begin{aligned} Pw^{\varepsilon} &= \frac{1}{T}\int_0^T \sin(2\pi t/T) - \text{sign}(\sin(2\pi t/T))^2 \\ &\quad + \cos(2\pi t/T) - \text{sign}(\cos(2\pi t/T))^2 dt \\ &= \frac{4}{T}\int_0^{T/4} \sin(2\pi t/T)^2 + 2\cos(2\pi t/T)^2 \\ &\quad - 2\sin(2\pi t/T) - \cos(2\pi t/T) + 2dt \\ &= 3 - \frac{4}{\pi}\big[-\cos(2\pi t/T) + \sin(2\pi t/T)\big]\Big|_0^{T/4} \\ &= 3 - \frac{8}{\pi}. \end{aligned}$$

Therefore, the signal $\varepsilon(t)$ is assumed to be a zero-mean noise uniformly distributed in the interval $[-\epsilon, \epsilon]$ with variance $\epsilon^2/12$ per real and imaginary components where $\epsilon = \sqrt{12Pw^{\varepsilon}} \approx 2.3329$. Let $f_{\varepsilon}(x)$ be the PDF of $\varepsilon(t)$. Hence, the PDF of $\eta(t) + \varepsilon(t)$ is given by

$$\begin{aligned} f_{\eta+\varepsilon}(x) &= \frac{1}{\sqrt{\pi N_0}} \exp\left(\frac{x^2}{N_0}\right) \circledast f_{\varepsilon}(x) \\ &= \frac{1}{\epsilon}\left(Q\left(\frac{x - \epsilon/2}{\sqrt{2N_0}}\right) + Q\left(\frac{x + \epsilon/2}{\sqrt{2N_0}}\right)\right) \end{aligned}$$

that represents the PDF of the addition of two random variables [22], and $\circledast$ stands for the linear convolution operation.

Let

$$\mathcal{G}(x) = \int_{\sqrt{2N_0}x/2}^{\infty} f_{\eta+\varepsilon}(\xi)d\xi$$

then, the error probability for metric proposal 1 is

$$P_e \leq \frac{2K}{M}\mathcal{G}\left(d_{\min}\sqrt{\frac{E_s}{N_0}}\right). \quad (42)$$

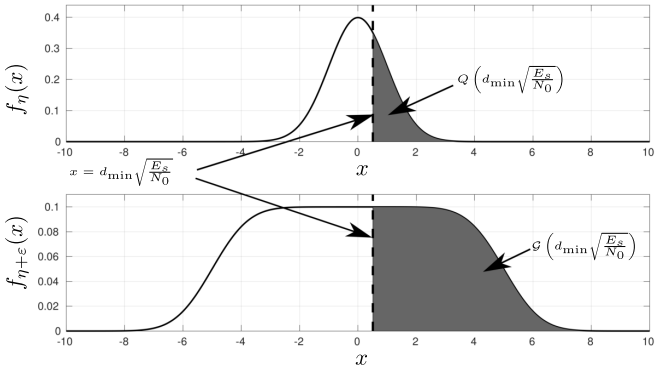

Fig. 6. Probability density function $f_\eta(x)$ [respectively, $f_{\eta+\varepsilon}(x)$] used to calculate error probability for the case depicted in Fig. 4 (respectively, Fig. 5).

TABLE IV
ESTIMATION OF $d^2_{\min}$ USING $N = 8$ SYMBOLS

Metric	M	K	$d^2_{\min}$	**Tight upper bound for** P_e
Trad.	256	256	2.0380	Eq. (41)
Prop. 1	256	256	2.0380	Eq. (42)
Prop. 2	256	256	1.9992	Eq. (41)

Fig. 6 provides a graphical depiction of the PDFs $f_\eta(x)$ and $f_{\eta+\varepsilon}(x)$. Note that P_e represents the sequence error probability rather than the symbol error probability. However, symbol error probability is often approximated by P_e for high values of E_s/N_0 since it is more probable that errors occur in a sequence with only one erroneous symbol [23, Ch. 3].

Table IV shows the parameters used to compute the error probability P_e tight upper bound for both the traditional metric and the metric proposals presented in this article. The value of $d^2_{\min}$ was estimated using N from 4 to 12 symbols. Results show variations of less than 10^{-9} for each metric. The signal space dimension $M = 2^N$ and the number of signal pairs with the same minimum distance K are shown for the case of $N = 8$.

V. RESULTS AND DISCUSSION

This section presents the theoretical and simulation results for the performance of the proposed receiver using the metrics described in Section III. The simulation parameters of the GFSK communication system are set as follows: a pulse $g(t)$ with $L = 3$ symbol periods and $BT = 0.5$; the modulation index is $h = 0.5$ and the VA has a traceback of 20 symbol periods. As a figure of merit, it is considered the E_s/N_o required to achieve a BER of 10^{-3}, this value is established in the Bluetooth core specification [5].

Fig. 7 depicts the simulated BER performance of the GFSK communication system using the proposed metrics as well as the performance of the system with the traditional metric, which matches the MLSE performance obtained from the results presented in [23, Ch. 3], by considering 3RC, $h = 0.5$, and $d^2_{\min} = 2$.

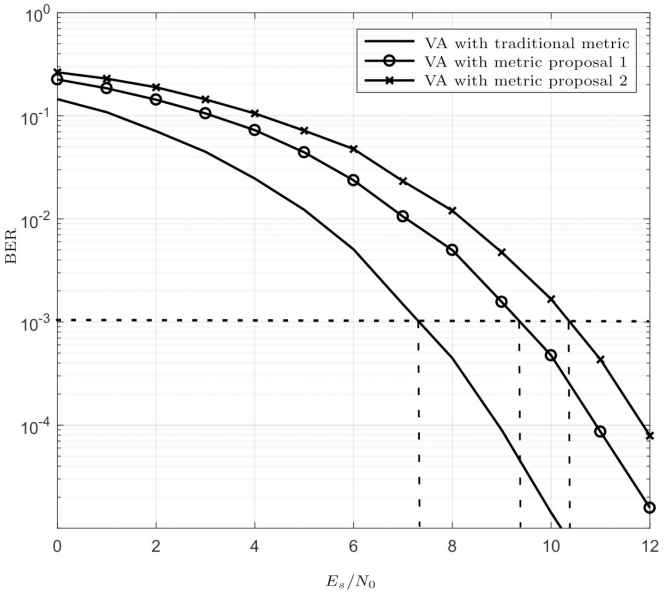

Fig. 7. BER performance of GFSK VA using the traditional and the proposed metrics.

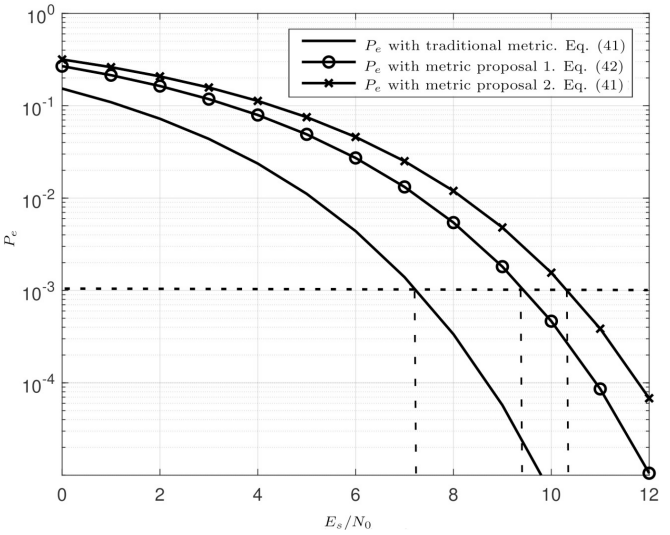

Fig. 8. Theoretical performance of GFSK VA using the traditional and proposed metrics.

Likewise, Fig. 8 shows the theoretical performance described by (41) and (42) for proposals 2 and 1, respectively. In this way, the simulation results validate the theoretical analysis since both are in good agreement.

It can be observed that the receiver system with the proposed metrics 1 and 2 exhibits a loss of 2 and 3 dB, respectively, when compared with the MLSE performance (traditional metric). However, if the computational complexity and the hardware resources presented in Table II are considered, it is very clear that the proposed metrics implies a significant reduction in hardware resources, since no subtractors and multipliers are required in both proposals. Furthermore, metric 2 is the best scheme in terms of required memory bits.

In addition, it is important to mention that the Bluetooth core specification [5] requires a sensitivity level of -70 dBm for a BER of 0.1%, which is achieved with $E_s/N_o = 21$ dB,

according to [24]. In this respect, and taking as a reference this E_s/N_o level, the proposals 1 and 2 show a gain, with respect to the specification requirements, equal to $21 - 9.5 = 11.5$ dB and $21 - 10.5 = 10.5$ dB, respectively.

VI. Conclusion

In this article, we proposed a novel GFSK Bluetooth receiver for IoT devices, which exhibits low complexity and close MLSE performance.

The reduction in complexity was achieved through a transformation of the received signal. This processing allows the use of two simplified metrics in the implementation of the VA. The proposed metrics attain a reduction of computational complexity and hardware resources.

The theoretical and simulation results show that the receiver using the metric proposal 2 has the most large-scale improvement in hardware resources required for its implementation in comparison with the traditional implementation used by VA. Specifically, there are no adders, subtractors, and multipliers involved. Furthermore, the required memory represents 0.31% of the memory bits employed by traditional metric when a *word* of 32 bits is considered. This remarkable hardware reduction implied a BER degradation of 3 dB with respect to MLSE performance. Because of the reduction in hardware resources and the coverage of the BER requirement for the Bluetooth core specification, proposal 2 is very attractive and feasible to be implemented in BLE-based IoT devices.

References

[1] J. Valencia-Velasco, R. Aldana-Lopez, and O. Longoria-Gandara, "Alternative Viterbi detection metrics for GFSK receivers: A hardware reduction approach," in *Proc. IEEE 10th Latin Amer. Conf. Commun. (LATINCOM)*, Nov. 2018, pp. 1–5.

[2] S. Chen, H. Xu, D. Liu, B. Hu, and H. Wang, "A vision of IoT: Applications, challenges, and opportunities with China perspective," *IEEE Internet Things J.*, vol. 1, no. 4, pp. 349–359, Aug. 2014.

[3] A. Zanella, N. Bui, A. Castellani, L. Vangelista, and M. Zorzi, "Internet of Things for smart cities," *IEEE Internet Things J.*, vol. 1, no. 1, pp. 22–32, Feb. 2014.

[4] M. Collotta, G. Pau, T. Talty, and O. K. Tonguz, "Bluetooth 5: A concrete step forward toward the IoT," *IEEE Commun. Mag.*, vol. 56, no. 7, pp. 125–131, Jul. 2018.

[5] *Bluetooth Core Specification, Version 5.1*, Bluetooth Special Interest Group, Kirkland, WA, USA, 2019.

[6] J. G. Proakis and M. Salehi, *Digital Communications*, 5th ed. San Diego, CA, USA: McGraw-Hill, 2008.

[7] J. P. Fonseka, "Soft-decision phase detection with Viterbi decoding for CPM signals," *IEEE Trans. Commun.*, vol. 47, no. 12, pp. 1802–1810, Dec. 1999.

[8] B. Xia, C. Xin, W. Sheng, A. Y. Valero-Lopez, and E. Sanchez-Sinencio, "A GFSK demodulator for low-IF Bluetooth receiver," *IEEE J. Solid-State Circuits*, vol. 38, no. 8, pp. 1397–1400, Aug. 2003.

[9] M. Kalkan and F. Keresteciogl u, "Zero-crossing based demodulation of minimum shift keying," *Turk. J. Elect. Eng. Comput. Sci.*, vol. 11, no. 2, pp. 75–94, 2003.

[10] T. Scholand and P. Jung, "Bluetooth receiver based on zero-crossing demodulation," *Electron. Lett.*, vol. 39, no. 4, pp. 397–398, Feb. 2003.

[11] L. Lampe, R. Schober, and M. Jain, "Noncoherent sequence detection receiver for Bluetooth systems," *IEEE J. Sel. Areas Commun.*, vol. 23, no. 9, pp. 1718–1727, Sep. 2005.

[12] N. Ibrahim, L. Lampe, and R. Schober, "Bluetooth receiver design based on Laurent's decomposition," *IEEE Trans. Veh. Technol.*, vol. 56, no. 4, pp. 1856–1862, Jul. 2007.

[13] N. M. Zayed and L. R. Carley, "Generalized partial response signalling and efficient MLSD using linear Viterbi branch metrics," in *Proc. Seamless Interconnection Univ. Services Glob. Telecommun. Conf. (GLOBECOM')*, vol. 1B, Dec. 1999, pp. 949–954.

[14] F. Xiong, *Digital Modulation Techniques*. Norwood, MA, USA: Artech House, Jan. 2006.

[15] J.-R. Lin, T. Talty, and O. K. Tonguz, "On the potential of Bluetooth low energy technology for vehicular applications," *IEEE Commun. Mag.*, vol. 53, no. 1, pp. 267–275, Jan. 2015.

[16] C. I. Votis, V. Christofilakis, and P. Kostarakis, "SIMO channel performance evaluation on indoor environment at 2.4 GHz," *Int. J. Electron.*, vol. 103, no. 4, pp. 648–666, 2016.

[17] T. S. Rappaport, *Wireless Communications: Principles and Practice*, 2nd ed. Upper Saddle River, NJ, USA: Prentice-Hall, 2002.

[18] T. Watteyne, S. Lanzisera, A. Mehta, and K. S. J. Pister, "Mitigating multipath fading through channel hopping in wireless sensor networks," in *Proc. IEEE Int. Conf. Commun.*, May 2010, pp. 1–5.

[19] L. R. Wilhelmsson, M. M. Lopez, and D. Sundman, "NB-WiFi: IEEE 802.11 and Bluetooth low energy combined for efficient support of IoT," in *Proc. IEEE Wireless Commun. Netw. Conf. (WCNC)*, Mar. 2017, pp. 1–6.

[20] G. D. Forney, "The Viterbi algorithm," *Proc. IEEE*, vol. 61, no. 3, pp. 268–278, Mar. 1973.

[21] D. J. S. Robinson, *An Introduction to Abstract Algebra*. Berlin, Germany: Walter de Gruyter, Aug. 2008.

[22] A. Papoulis, *Probability, Random Variables and Stochastic Processes*, 3rd ed. New York, NY, USA: McGraw-Hill, 1991.

[23] J. B. Anderson, T. Aulin, and C.-E. Sundberg, *Digital Phase Modulation*. New York, NY, USA: Plenum Press, 1986.

[24] B. A. Georgescu, J. K. Nakaska, R. G. Randall, and J. W. Haslett, "A 0.18/spl μ/m CMOS Bluetooth frequency synthesizer for integration with a Bluetooth SoC reference platform," in *Proc. 3rd IEEE Int. Workshop Syst. Chip Real-Time Appl.*, Jul. 2003, pp. 258–263.

Jose Valencia-Velasco (Member, IEEE) was born in Guadalajara, Mexico, in 1980. He received the B.Sc. degree in electronics engineering from Centro de Enseñanza Tecnica Industrial (CETI), Guadalajara, Mexico, in 2004, and the M.Sc. degree in electronic design from the Instituto Tecnológico y de Estudios Superiores de Occidente, Tlaquepaque, Mexico, in 2014, where he is currently pursuing the Ph.D. degree.

Since 1999, he has been a Full-Time Professor with the Electronics Department, CETI. His research interests include digital signal processing and digital communications.

Omar Longoria-Gandara (Member, IEEE) was born in Delicias, Mexico, in 1971. He received the B.Sc. degree in electronics and communications from the Instituto Tecnológico y de Estudios Superiores de Monterrey (ITESM-Mty), Monterrey, Mexico, in 1993, the M.Sc. degree in electrical engineering specialized in communications from CINVESTAV-IPN, Mexico City, Mexico, in 1998, and the Ph.D. degree with research in time invariant/variant MIMO channel estimation, radio channel modeling, and space-time block codes from CINVESTAV-IPN in 2010.

From 1998 to 2006, he was with the Electrical Engineering Department, ITESM, Guadalajara, Mexico, as a Full Time Professor and from 2004 to 2006 he was in charge of the department. He is currently with the Electronics, Systems and IT Department, ITESO University, Tlaquepaque, Mexico. His research interests include MIMO channel estimation, performance and analysis of high-speed interconnect circuits, MIMO digital precoding and implementation of embedded communications algorithms using hardware description languages.

Rodrigo Aldana-Lopez (Member, IEEE) was born in Guadalajara, Mexico, in 1993. He received the B.Sc. degree in electronics engineering from the Instituto Tecnológicoy de Estudios Superiores de Occidente, Tlaquepaque, Mexico, in 2016. He is currently pursuing the Ph.D. degree with the Department of Computer Science and Systems Engineering, University of Zaragoza, Zaragoza, Spain.

His research interests include real-time constrained robotics and machine learning, nonuniform sampling, and communication protocols design for distributed systems.

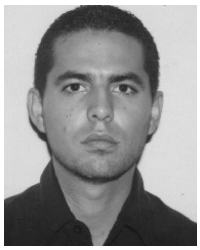

Luis Pizano-Escalante (Member, IEEE) was born in Guadalajara, Mexico, in 1983. He received the B.Sc. degree in electronics and communications from the University of Guadalajara, Guadalajara, in 2007, and the M.Sc. degree in electrical engineering and the Ph.D. degree in electrical engineering (with a specialization in digital signal processing for communications) from the Centro de Investigación y de Estudios Avanzados del Instituto Politécnico Nacional, Mexico City, Mexico, in 2010 and 2014, respectively.

He is currently with the Electronics, Systems and IT Department, Instituto Tecnológico y de Estudios Superiores de Occidente, Tlaquepaque, Mexico. His research interests include digital signal processing, performance and analysis of HSI circuits, MIMO digital precoding, computer architecture, and embedded systems.